J. Phys. B: Atom. Molec. Phys., Vol. 12, No. 20, 1979. Printed in Great Britain

Effective potential theory of e^-–H_2 rotational excitation

E Ficocelli Varracchio

Istituto di Chimica Generale, Centro di Studio per la Chimica dei Plasmi, CNR Università di Bari, Via Amendola 173, 70126 Bari, Italy

Received 20 February 1979, in final form 9 May 1979

Abstract. A recently developed 'effective potential' formalism is applied to the e^-–H_2 elastic scattering and rotational excitation processes. The partial-wave analysis of the 'optical' and 'transition' potentials of the theory, relative to elastic and inelastic processes, respectively, is developed. The first quantity enters into a (small) set of coupled integral equations, which are solved numerically by a non-iterative technique. The second quantity is used to evaluate a matrix element, directly related to the T-matrix of inelastic transitions. A comparison of the results shows good agreement with exact close-coupling calculations, particularly for inelastic processes, which are dominated by higher partial waves.

1. Introduction

In a recent paper (Ficocelli Varracchio 1977, to be referred to as I) an 'effective potential' formulation of vibro-rotational excitation in particle–diatom scattering has been outlined. This is based on a field-theoretic (FT) description of scattering and it leads naturally to '*ab initio*' definition of both 'optical' and 'transition' potentials, characterising elastic and inelastic processes, respectively. Exact closed equations have been given in I for the above mentioned quantities and explicit approximations, of the second order in the subsystems interaction potential, suggested (see also Csanak *et al* 1974).

The purpose of this paper is to present the first numerical application of the FT theory to low energy electron–diatom rotational excitation. To test the theory, the H_2 molecule has been chosen with an interaction potential suggested by Lane and Geltman (1967), who have performed extensive close-coupling (CC) calculations. In order to get a deeper understanding of the validity of the present approach, a comparison has also been made with the results of the distorted-wave (DW) approximation, for which explicit computations have been carried out. No attempt has been made instead, at this stage, to compare with experimental data. This is mostly a matter of accuracy of the potential used in the calculations and, as such, outside the spirit of the present paper.

In the next section the fundamental equations of the theory are briefly reviewed, with particular emphasis on the relevant aspects of the partial-wave analysis. This leads to a set of coupled integral equations, with non-local and energy-dependent kernels, which are thoroughly investigated, from a computational point of view, in § 3. The results obtained are analysed and compared to both the CC and DW values in § 4, which is followed by a concluding summary, in § 5.

0022-3700/79/203427+14$01.00

2. Equations of the theory

Since an extensive account of the FT approach has already been given in I, in this section we shall simply summarise the relevant formulae, referring to I for details.

In the present formalism elastic and inelastic scattering are treated separately. The first one is related to the solution of the integral (Dyson's) equation (we shall adopt, wherever convenient, an abstract vector space notation, thereby omitting integration signs)

$$|f^i_{k_i}\rangle = |\Phi_{k_i}\rangle + g(\epsilon_i)\Sigma^i(\epsilon_i)|f^i_{k_i}\rangle \tag{1}$$

with $\epsilon_i = \hbar^2 k_i^2/2m$ the energy of the impinging electron and 'i' labelling the initial vibro-rotational state of the target. $\Sigma^i(\epsilon_i)$ is the non-local and energy-dependent 'optical' potential of elastic scattering, which contains information on all molecular states different from 'i'; Φ and $g(\epsilon)$ represent a plane wave and the free-particle Green's function, respectively. Information on inelastic transitions are obtained by calculating matrix elements of the type

$$T_{fk_f;ik_i} = -2\pi i\delta(\epsilon_f - \epsilon_i + \omega_{fi})\langle f^{i(-)}_{k_f}|V_{f\leftarrow i}(\tfrac{1}{2}(\epsilon_f + \epsilon_i))|f^{i(+)}_{k_i}\rangle \tag{2}$$

with $\omega_{fi} = \omega_f - \omega_i$ being the energy involved in the inelastic process. The $f^{(+)}$ and $f^{(-)}$ orbitals are solutions of equation (1), satisfying outgoing- and incoming-wave boundary conditions, respectively. The $V_{f\leftarrow i}$ 'transition' potential represents the second effective potential of the theory and, in analogy to $\Sigma^i(\epsilon)$, it is non-local and energy dependent.

For numerical applications, a partial-wave analysis of (1) is needed. By adopting a space-fixed reference frame (Arthurs and Dalgarno 1960) this is readily obtained, in conventional notation, as

$$|f^{iJ}_{ll'k_i}\rangle = |F_{l'}\rangle\delta_{ll'} + \sum_{l''} g_{l''}(\epsilon_i)\Sigma^{iJ}_{l'l''}(\epsilon_i)|f^{iJ}_{ll''k_i}\rangle. \tag{3}$$

In the coordinate representation, the (outgoing-wave) Green's function becomes

$$g^{(+)}_l(r, r'; \epsilon_i) = -\frac{2m}{\hbar^2 k_i} F_l(k_i r_<) H^{(+)}_l(k_i r'_>) \tag{4}$$

with F_l and $H^{(+)}_l$ the regular and irregular spherical Bessel's functions, respectively. The optical potential is similarly given by

$$\Sigma^{iJ}_{l'l''}(r, r'; \epsilon_i) = \sum_{m_i m_{l'} m_{l''}} \int d\hat{\boldsymbol{r}}\, d\hat{\boldsymbol{r}}'\, rr'\langle j_i l' m_i m_{l'}|JM\rangle Y^*_{l'm_{l'}}(\hat{\boldsymbol{r}})\Sigma^i(\boldsymbol{r}, \boldsymbol{r}'; \epsilon_i) Y_{l''m_{l''}}(\hat{\boldsymbol{r}}')$$
$$\times \langle j_i l'' m_i m_{l''}|JM\rangle \tag{5}$$

with $\langle \ldots|\ldots\rangle$ a 3-j symbol (Brink and Satchler 1971). The computations of the present paper have been performed within the $\Sigma^i \cong \Sigma^{i(1)}$ approximation of I, that can conveniently be written, in terms of partial-wave components, as

$$\Sigma^{iJ(1)}_{l'l''}(r, r'; \epsilon_i) = {}^1\Sigma^{iJ}_{l'l''}(r, r'; \epsilon_i) + {}^2\Sigma^{iJ}_{l'l''}(r, r'; \epsilon_i). \tag{6}$$

The ${}^1\Sigma$ and ${}^2\Sigma$ terms on the right-hand side of equation (6) are expressions of the first and second order, respectively, in the system interaction potential. By freezing the vibrational degree of freedom, this last quantity can be written, as usual, in the form

$$V(\boldsymbol{r}, \hat{\boldsymbol{R}}) = \sum_\lambda v_\lambda(r) P_\lambda(\hat{\boldsymbol{r}} \cdot \hat{\boldsymbol{R}}) \tag{7}$$

with $\hat{\boldsymbol{R}}$ denoting the direction of the molecular axis. Using (7) and (5), it can then be readily shown that the two terms in (6) become

$$ {}^1\Sigma^{iJ}_{l'l''}(r, r'; \epsilon_i) = \delta(r-r')\left(\frac{4\pi}{2J+1}\right)^{1/2} \sum_{\lambda} v_\lambda(r) Z(l'J\lambda j_i; j_i l'') \tag{8} $$

$$ {}^2\Sigma^{iJ}_{l'l''}(r, r'; \epsilon_i) = \frac{4\pi}{(2J+1)} \sum_{\substack{j_n \neq j_i \\ L\lambda\lambda'}} v_\lambda(r) G_L(r, r'; \epsilon_n) v_{\lambda'}(r') \frac{(2j_i+1)}{(2j_n+1)} Z(l'J\lambda j_n; j_i L) Z(l''J\lambda' j_n; j_i L). \tag{9} $$

The Z coefficients are given by

$$ Z(lJ\lambda j_n; j_i L) = \frac{(-l)^{l+L-\lambda}}{(2\lambda+1)} [4\pi(2l+1)(2J+1)(2j_n+1)]^{1/2} \times \langle j_i \| \boldsymbol{Y}_\lambda \| j_n \rangle \langle l \| \boldsymbol{Y}_\lambda \| L \rangle W(lJ\lambda j_n; j_i L) \tag{10} $$

and the $\langle \ldots \| \ldots \| \ldots \rangle$ reduced matrix elements and Racah W functions are defined as in Brink and Satchler. The G_L Green's function in (9) is formally related to the solutions of (3), by

$$ G_l(r, r'; \epsilon) = \lim_{\eta \to 0^+} \sum_{k'l'} \frac{f^{iJ}_{ll'k'}(r) f^{iJ*}_{ll'k'}(r')}{\epsilon - \epsilon' + i\eta} \tag{11} $$

and it can be explicitly obtained, to different degrees of accuracy, as we shall see later in detail. The partial-wave analysis of the transition potential proceeds along similar lines, with the definition of

$$ V^J_{l'j_f;\, l''j_i}(r, r'; \epsilon) = \sum_{\substack{m_i m_f \\ m_{l'} m_{l''}}} \int d\hat{\boldsymbol{r}}\, d\hat{\boldsymbol{r}}'\, rr' \langle j_f l' m_f m_{l'} | JM \rangle Y^*_{l'm_{l'}}(\hat{\boldsymbol{r}}) V_{f \leftarrow i}(\boldsymbol{r}, \boldsymbol{r}'; \epsilon) Y_{l''m_{l''}}(\hat{\boldsymbol{r}}') \times \langle j_i l'' m_i m_{l''} | JM \rangle. \tag{12} $$

In analogy to the optical potential, the $V^{(1)}_{f \leftarrow i}$ approximation of I has been adopted for the calculations of this paper or, in a convenient separation of terms

$$ V^{J(1)}_{l'j_f;\, l''j_i}(r, r'; \epsilon) = {}^1V^J_{l'j_f;\, l''j_i}(r, r'; \epsilon) + {}^2V^J_{l'j_f;\, l''j_i}(r, r'; \epsilon) + {}^3V^J_{l'j_f;\, l''j_i}(r, r'; \epsilon). \tag{13} $$

The three quantities on the right-hand side of equation (13) are given explicitly by

$$ {}^1V^J_{l'j_f;\, l''j_i}(r, r'; \epsilon) = \delta(r-r')\left(\frac{4\pi(2j_f+1)}{(2j_i+1)(2J+1)}\right)^{1/2} \sum_{\lambda} v_\lambda(r) Z(l'J\lambda j_i; j_f l'') \tag{14} $$

$$ {}^2V^J_{l'j_f;\, l''j_i}(r, r'; \epsilon) = \frac{4\pi}{(2J+1)} \sum_{\substack{j_n \neq j_i, j_f \\ L\lambda\lambda'}} v_\lambda(r) G_L(r, r'; \epsilon - \omega_{ni} + \tfrac{1}{2}\omega_{fi}) \times v_{\lambda'}(r') \frac{(2j_f+1)}{(2j_n+1)} Z(l'J\lambda j_n; j_f L) Z(l''J\lambda' j_n; j_i L) \tag{15} $$

$$ {}^3V^J_{l'j_f;\, l''j_i}(r, r'; \epsilon) = \frac{4\pi(2j_f+1)}{(2j_i+1)(2J+1)} \sum_{\lambda\lambda' L} v_\lambda(r) G_L(r, r'; \epsilon - \tfrac{1}{2}\omega_{fi}) \times v_{\lambda'}(r') [Z(l'J\lambda j_f; j_f L) - Z(l'J\lambda j_i; j_i L)] Z(l''J\lambda' j_f; j_i L) \tag{16} $$

thus showing that ${}^1V$ is of the first order in the interaction potential, while ${}^2V$ and ${}^3V$ are second-order expressions. Equations (8), (9) and (14)–(16) constitute the working approximations to the effective potentials used in this paper and these can be immediately generalised, if necessary, to include the target vibrational degree of freedom (see I for details).

The elastic and inelastic T-matrix elements immediately follow from equations (1) and (2), respectively. In our approximation scheme, they become explicitly

$$T^J(l'j_i; lj_i) = -\frac{4m}{i\hbar^2 k_i} \sum_{l''} \langle F_{l'} | \Sigma^{iJ(1)}_{l'l''}(\epsilon_i) | f^{iJ(+)}_{ll''k_i} \rangle \tag{17}$$

$$T^J(l'j_f; lj_i) = -\frac{4m}{i\hbar^2 k_i} \sum_{l''} \langle f^{iJ(-)}_{ll'k_f} | V^{J(1)}_{l'j_f; l''j_i}(\tfrac{1}{2}(\epsilon_f + \epsilon_i)) | f^{iJ(+)}_{ll''k_i} \rangle. \tag{18}$$

With the above definitions of the T-matrix elements, expressions for the various cross sections of interest can be obtained in the usual fashion. In order to establish a convenient notation, we shall define the following partial cross sections

$$\sigma^J_{l'l}(j_f, j_i) = \frac{\pi}{k_f^2} \frac{(2J+1)}{(2j_i+1)} |T^J(l'j_f; lj_i)|^2 \tag{19}$$

in terms of which total cross sections, characterising rotational excitation processes, become

$$\sigma(j_f, j_i) = \sum_{Jll'} \sigma^J_{l'l}(j_f, j_i). \tag{20}$$

To conclude this section, we briefly review the Lane and Geltman interaction potential used in the computations. This is made up of three terms, or specifically

$$V(r, R) = \sum_{\lambda=0}^{4} v^B_\lambda(r) P_\lambda(\hat{\boldsymbol{r}} \cdot \hat{\boldsymbol{R}}) \tag{21}$$

with

$$v^B_0(r) = v^W_0(r) B(r) + v_{LR0}(r) \tag{22}$$

$$v^B_2(r) = v^W_2(r) B(r) + v_{LR2}(r) \tag{22a}$$

$$v^B_4(r) = v^W_4(r) B(r). \tag{22b}$$

In (22)–(22b), the v^W_i represent the 'short-range' portions of the interaction, obtainable from Wang's wavefunction for H_2 (Wang 1928). The 'long-range' v_{LR0} and v_{LR2} terms are defined by

$$v_{LR0}(r) = -(\alpha/2r^4) C(r) \tag{23}$$

$$v_{LR2}(r) = -(\alpha'/2r^4 + Q/r^3) C(r) \tag{23a}$$

with

$$C(r) = 1 - \exp[-(r/R)^p]. \tag{23b}$$

Finally, the $B(r)$ cut-off function is given by

$$B(r) = \begin{cases} \exp[-B(s/2 - r)] & \text{for } r \leq s/2 \\ 1 & \text{for } r > s/2. \end{cases} \tag{24}$$

The values of the parameters appearing in equations (23)–(24) are listed in table 1 and we refer to the original paper for a discussion of the various terms of (21) and more details on the accuracy of the potential. The computations have been performed by using atomic units, with the scattering energy, k^2, given in rydbergs (Ryd).

Table 1. Values of the parameters used in the interaction potential (equations (21)–(24)).

$B(r)$	$C(r)$	v_0^B	v_2^B
$B=-2{\cdot}50\ a_0^{-1}$ $s=1{\cdot}40\ a_0$	$p=6$ $R=1{\cdot}8\ a_0$	$\alpha=5{\cdot}5\ a_0^3$	$\alpha'=1{\cdot}38\ a_0^3$ $Q=0{\cdot}49\ ea_0^2$

3. Numerical scheme of solution

It should be evident from the discussion in the previous section that the most important step in the numerical implementation of the FT scheme is represented by the solution of the partial-wave Dyson's equations, (3). By defining

$$\gamma_{l'l''}(r, r') = \delta(r-r')\left(\frac{4\pi}{2J+1}\right)^{1/2} \sum_{\lambda} v_\lambda(r) Z(l'J\lambda j_i; j_i l'') \tag{25}$$

$$\alpha_{l'j_nL}(r) = \frac{4\pi(2j_i+1)}{(2J+1)(2j_n+1)} \sum_{\lambda} v_\lambda(r) F_L(k_n r) Z(l'J\lambda j_n; j_i L) \tag{26}$$

$$\beta_{l''j_nL}(r') = -\frac{2m}{\hbar^2 k_n} \sum_{\lambda'} v_{\lambda'}(r') H_L^{(+)}(k_n r') Z(l''J\lambda' j_n; j_i L) \tag{27}$$

the set of coupled-integral equations to be solved can generally be written as

$$f^{iJ}_{ll'k}(r) = F_{l'}(kr)\delta_{ll'} + \sum_{l''} \int \mathrm{d}r'\, \mathrm{d}r''\, g_{l'}(r, r'; \epsilon) \times \left(\gamma_{l'l''}(r', r'') + \sum_{\substack{j_n L \\ (j_n \neq j_i)}} \alpha_{l'j_nL}(r'_<)\beta_{l''j_nL}(r''_>)\right) f^{iJ}_{ll''k}(r''). \tag{28}$$

The kernel in (28) is of the separable type and we have, therefore, been able to implement a non-iterative technique to solve it (Burke and Seaton 1971, Thomas 1973). In defining the α and β functions, equations (26) and (27), respectively, we have implicitly enforced the $G_L \cong g_L$ approximation on the one-particle Green's function (compare equations (9), (11) and (4)). We are not limited to this choice, however, and to next order a 'distorted-wave' Green's function, g_L^{DW}, can be readily evaluated by simply keeping the first term within brackets in (28). If we further neglect coupling effects in γ, g_L^{DW} can conveniently be obtained in closed form as

$$g_L^{\mathrm{DW}}(r, r'; \epsilon_n) = -\frac{2m}{\hbar^2 W_n} R_L(k_n r_<) I_L(k_n r'_>). \tag{29}$$

In equation (29) W_n is the Wronskian of the R_L (regular) and I_L (irregular) functions,

defined explicitly by

$$R_L(k_n r) = F_L(k_n r) + \int \mathrm{d}r'\, \mathrm{d}r''\, g_L(r, r'; \epsilon_n)\gamma_{LL}(r', r'')R_L(k_n r'') \tag{30}$$

$$I_L(k_n r) = H_L^{(+)}(k_n r) + \int \mathrm{d}r'\, \mathrm{d}r''\, g_L(r, r'; \epsilon_n)\gamma_{LL}(r', r'')I_L(k_n r''). \tag{31}$$

With such a representation for g_L^{DW}, the form of the α and β functions remains unchanged under the $g_L \to g_L^{\mathrm{DW}}$ transformation provided we perform the substitutions in (26) and (27)

$$F_L(k_n r) \to R_L(k_n r) \tag{32}$$

$$\frac{1}{k_n} H_L^{(+)}(k_n r) \to \frac{1}{W_n} I_L(k_n r). \tag{32a}$$

To test the effect of the improvement (or renormalisation) in the representation of G_L quantitatively, we can consider its influence on the 'loss of flux' into the inelastic channels. If we define, in other words, the function

$$\chi_{j_n}^{iJ}(r; \epsilon) = -\mathrm{Im} \sum_{l'l''} \Sigma_{l'l''}^{iJ(1)}(r, r; \epsilon)$$

$$= -\mathrm{Im} \sum_{l'l''L} (\gamma_{l'l''}(r, r) + \alpha_{l'j_nL}(r)\beta_{l''j_nL}(r)) \tag{33}$$

this quantity is related, for each value of r, to the energy lost by the incident electron, due to virtual excitation of the j_nth level, in the Jth total angular momentum state. Plots of the $\chi_{j_n}^{iJ}$ function are given in figure 1 for the $j_i = 0$ entrance channel, at two different energies and with both a plane-wave and a distorted-wave approximation to G_L. This figure clearly shows that $\chi_{j_n}^{iJ}$ is strongly peaked at the position of the nuclei and that the introduction of the distorted waves in the optical potential has simply the effect of decreasing its imaginary component by a few per cent. That this effect is small overall is also indicated by a comparison, in table 2, of the $\sigma_{11}^{1}(0, 0)$ (see equation (19)) partial cross sections obtained in the two approximations. On the basis of the above results we have not found it necessary to consider higher order schemes for G_L, and we have used, in this paper, the $G_L \cong g_L^{\mathrm{DW}}$ approximation in our definition of the α and β functions (see equations (26), (27), (32) and (32a)).

We turn next to a consideration of the total number of coupled equations that derive from the non-iterative solution of (28). From the definition of the Z coefficient, equation (10), the following triangular conditions hold

$$|J - j_i| \leqslant l, l', l'' \leqslant J + j_i \tag{34}$$

with only waves of the same parity, $(-1)^l$, being coupled to each other, since we are considering a homonuclear molecule. For every allowed value of the electron's orbital angular momentum 'l', each (j_n, L) pair produces one additional coupled equation. An upper limit to this number derives from the triangular conditions (obtainable from equations (9) and (10))

$$|j_i - \lambda| \leqslant j_n \leqslant j_i + \lambda \tag{35}$$

$$|J - j_n| \leqslant L \leqslant J + j_n. \tag{35a}$$

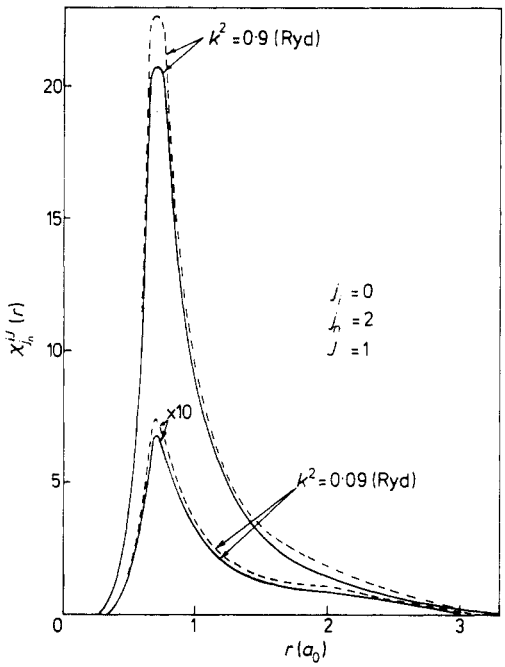

Figure 1. Plots of the 'loss of energy' into the $j_n = 2$ channel, with H_2 initially in the $j_i = 0$ rotational state. The full and broken curves have been calculated, at each energy, with distorted and plane-wave approximations to the full Green's function, respectively (see text).

Table 2. Values of the $\sigma^1_{11}(0,0)(a_0^2)$ partial cross sections obtained in the plane-wave (g_l) and distorted-wave (g_l^{DW}) approximations to the one-particle Green's function in $^2\Sigma$.

k^2(Ryd)	g_l	g_l^{DW}
0·09	5·898	5·652
0·9	14·175	14·088

Besides, j_n and L must have $(-1)^{j_i}$ and $(-1)^l$ parities, respectively, again on account of the homonuclear nature of the target. The total number of coupled equations is then given by

$$N = \Delta l\left(\sum_{j_n} N_{j_nL} + 1\right) \tag{36}$$

where Δl represents the allowed range of l values (obtainable from (34)) and N_{j_nL} is the total number of L states, associated with each j_n, according to (35a). Our calculations have shown that, for the H_2 molecule, only the lowest L value need be considered for every j_n, therefore yielding $N_{j_nL} = 1$. Moreover, numerical experimentation has shown that the summation over j_n in (28) is very rapidly convergent, so that, for practical purposes, the value of N, in (36), is very close to Δl. To substantiate this point, we are plotting in figure 2 the local imaginary component of the optical potential, $\chi^{iJ}_{j_n}$, with $j_i = 0$, $J = 1$ and at an energy of 1·5 Ryd. It can be seen from the figure that the loss of

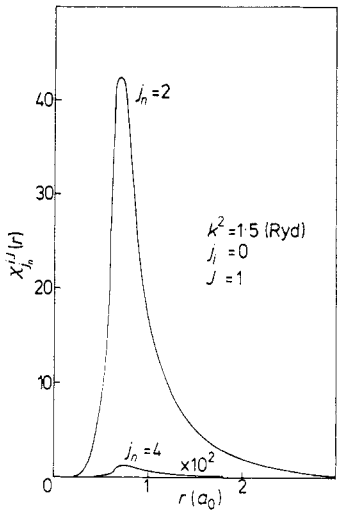

Figure 2. Plots of the 'loss of energy' into the $j_n = 2$ and $j_n = 4$ channels, respectively, at $k^2 = 1{\cdot}5$ (Ryd) and with H_2 initially in the $j_i = 0$ rotational state.

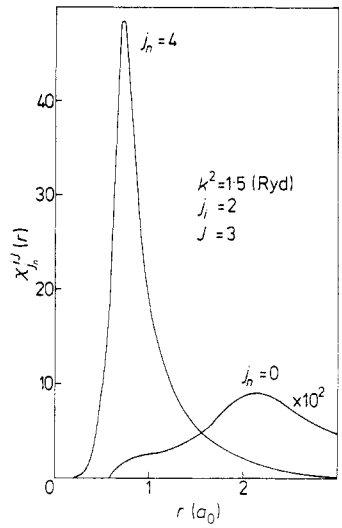

Figure 3. Plots of the 'loss of energy' into the $j_n = 0$ and $j_n = 4$ channels, respectively, at $k^2 = 1{\cdot}5$ (Ryd) and with H_2 initially in the $j_i = 2$ rotational state.

flux into the $j_n = 2$ state is two orders of magnitude bigger than in the $j_n = 4$ level. These same results have been verified at different energies and for different values of J. In figure 3, the $\chi^{iJ}_{j_n}$ function, for $j_i = 2$ and $J = 3$, is given, showing the relative influence of the $j_n = 0$ and $j_n = 4$ intermediate states. Aside from a displacement of the maxima of the two curves, it is seen that the lowest state gives a negligible contribution compared to the $j_n = 4$ level. This is partly due to the bigger energy denominator associated with the superelastic $j_i = 2 \rightarrow j_n = 0$ intermediate process (see equation (27)). In summary, converged computations have been performed by keeping only the $(j_i + 2)$ state for processes involving $j_i = 0, 1$ and both the $(j_i + 2)$ and $(j_i - 2)$ levels in the remaining cases.

The determination of the T matrix of the inelastic processes does not require any particular consideration. We simply point out that, as shown by (18) and (14)–(16), this involves solving Dyson's equation at two energies (and with different boundary conditions) and performing a double integration.

4. Results

4.1. Elastic scattering

We shall consider, first, the elastic scattering results, obtained by solving equation (28), with outgoing-wave boundary conditions. It has already been pointed out by Lane and Geltman that elastic processes are mainly due to $l = 0 \rightarrow l' = 0$ (s-wave) transitions, while $l = 1 \rightarrow l' = 1$ (p-wave) starts contributing only at higher energies ($k^2 \geq 0{\cdot}3$ Ryd). Our elastic scattering results, therefore, will depend to a large extent on the ability of $\Sigma^{(1)}$ to represent correctly the scattering in the penetrating s waves. If only the $^1\Sigma$ term is retained in the optical potential, equation (6), the familiar DW expression for elastic scattering, is recovered. $^2\Sigma$ represents, then, the second-order correction to the DW

theory. We have performed computations both by retaining the full $^2\Sigma$ quantity and by simply keeping its non-local imaginary component, e.g. $\mathrm{Im}(^2\Sigma)$. The results so obtained for the $\sigma^0_{00}(0, 0)$ partial cross section are compared to the exact CC values in figure 4. While the two FT calculations agree at higher energies ($k^2 \geqslant 1{\cdot}0$ Ryd), at lower energies the curve corresponding to $\Sigma^{(1)} = {}^1\Sigma + \mathrm{Im}(^2\Sigma)$ is in much better agreement with the exact CC values. This same trend is characteristic of all the $\sigma^J_{00}(j_i, j_i)$ partial cross sections investigated and we must conclude, therefore, that the second-order term in the optical potential is an overcorrection to the simple $^1\Sigma$ static quantity, in connection with the computation of s-wave scattering. These have consequently been calculated in this paper by enforcing the $\Sigma^{(1)} = {}^1\Sigma + \mathrm{Im}(^2\Sigma)$ approximation, that numerically is not very far from the DW results. The situation is completely different for the less penetrating p waves, as shown in figure 5 for $\sigma^1_{11}(0, 0)$. Here the full $\Sigma^{(1)}$ gives good agreement with the exact CC values, particularly at lower energies. The cross section is slightly overestimated at higher energies, where the DW and $\Sigma^{(1)}$ approximations are again in agreement. Total elastic cross sections, along with s- and p-wave partial contributions, are plotted in figures 6 and 7, for $j_i = 0$ and $j_i = 1$, respectively. A more extensive

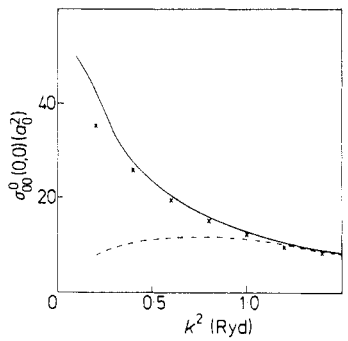

Figure 4. Comparison of s-wave cross sections: the full and broken curves have been computed within the $^1\Sigma + \mathrm{Im}(^2\Sigma)$ and $^1\Sigma + {}^2\Sigma$ approximations to the optical potential, respectively. Crosses are the exact CC results.

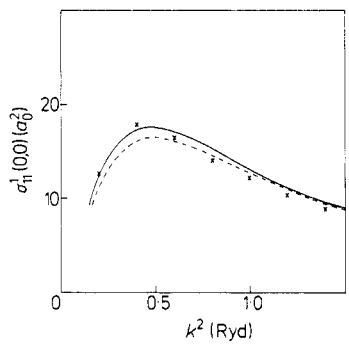

Figure 5. Comparison of p-wave cross sections: the full and broken curves have been computed within the $^1\Sigma + {}^2\Sigma$ and $^1\Sigma$ approximations to the optical potential, respectively. Crosses are the exact CC results.

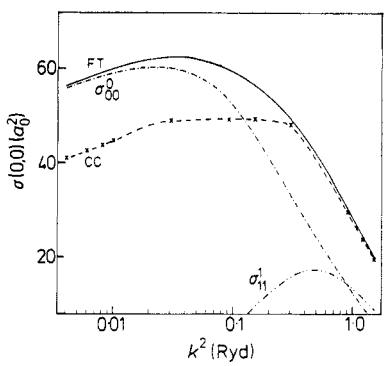

Figure 6. Comparison of the FT and CC $\sigma(0, 0)$ elastic cross sections. Also shown are s- and p-wave partial contributions.

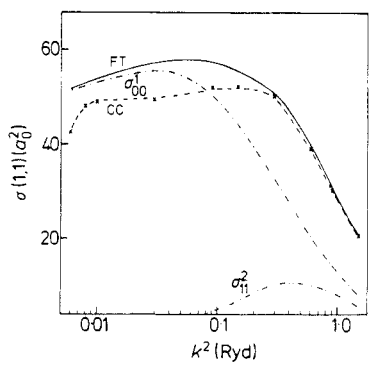

Figure 7. Comparison of the FT and CC $\sigma(1, 1)$ elastic cross sections. Also shown are s- and p-wave partial contributions.

comparison of data is presented in table 3. We can generally say that, in our scheme of calculation, the FT theory is in good agreement with CC for $k^2 \geqslant 0{\cdot}3$ Ryd, while overestimates of up to 30–35% can be expected at lower energies.

Table 3. Comparison of the FT and CC total elastic cross sections (in a_0^2).

k^2(Ryd)	$\sigma(0,0)$	$\sigma(1,1)$	$\sigma(2,2)$	$\sigma(3,3)$
0·03	62·584†	57·349	58·966	59·206
	49·110	49·358	49·287	49·273
0·09	59·879	57·382	57·653	57·700
	51·259	51·874	51·701	51·663
0·15	56·357	55·287	55·543	54·939
	51·218	52·252	51·955	51·900
0·3	49·939	50·899	50·443	49·400
	48·338	50·044	49·558	49·463
0·6	38·559	39·523	38·683	38·488
	37·613	39·137	38·704	38·608
0·9	29·954	30·784	28·874	29·966
	29·276	30·401	30·082	29·995
1·2	24·083	24·792	23·533	24·064
	23·693	24·569	24·319	24·230
1·5	20·027	20·979	19·572	19·915
	19·814	20·536	20·329	20·236

† The upper (lower) number, for each energy, is the FT (CC) value.

4.2. Inelastic scattering

Before starting a detailed analysis of rotational excitation, it is worth pointing out that s waves, fundamental for elastic scattering, do not contribute at all to inelastic processes, as can be readily verified from equations (14)–(16) and the definition of the Z coefficient, (10). A second point of interest is that, contrary to the elastic scattering case, the FT inelastic formula, equation (18), does not reduce to the DW theory, even in a lowest order approximation to the transition potential (i.e. $V^J_{l'j_f;l''j_i} \cong {}^1V^J_{l'j_f;l''j_i}$). This is due to the fact that the $f^{(-)}$ orbital of (18) is determined by an optical potential which is related to the j_i 'initial' state of the transition. The effect of the j_f 'final' state comes through the ${}^3V$ term given by equation (16). The ${}^2V$ quantity, equation (15), represents, finally, the contribution to inelastic processes due to a two-step excitation mechanism. On this basis we shall refer, in the following, to the ${}^1V$, ${}^2V$ and ${}^3V$ terms as the direct transition (DT), the transition polarisation (TP) and the final-state correction (FSC), respectively. The corresponding contributions to the cross sections will be labelled as σ^{DT}, σ^{TP} and σ^{FSC}, in turn.

We consider first $j_i \to j_i + 2$ inelastic processes, that show a characteristic predominance of the p wave ($l = l' = 1$ in (18)). As can be inferred from figure 5, the corresponding $f_{ll'}$ orbitals should be reasonably well computed in the $\Sigma^{(1)}$ approximation to the optical potential and we expect, therefore, good agreement with the CC calculations. Figure 8 shows some numerical results for the $\sigma(3,1)$ cross section, thus confirming our expectations. The FT values are, in fact, very close to the CC computations and definitely represent an improvement over the DW theory, that lies lower in the whole energy range. In order to investigate the effect of Σ on inelastic transitions, we have calculated $\sigma(3,1)$ by using in (18) f orbitals obtained with both the ${}^1\Sigma$ and

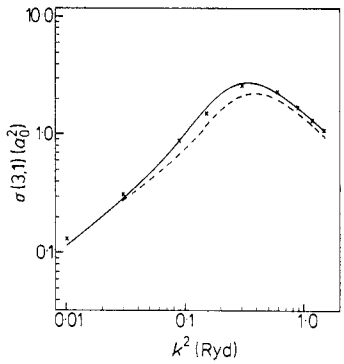

Figure 8. Comparison of $\sigma(3, 1)$ cross sections: the full and broken curves are the FT and DW results, respectively. Crosses are the exact CC values.

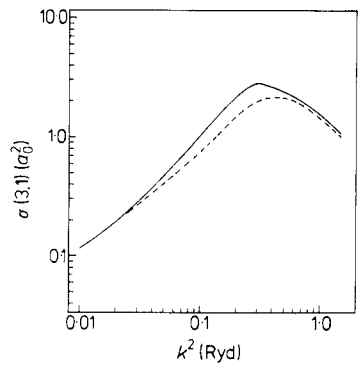

Figure 9. Inelastic $\sigma(3, 1)$ cross sections: the full curve corresponds to Dyson's orbitals computed within the $^1\Sigma + {}^2\Sigma$ approximation to the optical potential, while $^1\Sigma$ has been used for the broken curve.

($^1\Sigma + {}^2\Sigma$) approximations to the optical potential. The corresponding curves are plotted in figure 9, showing that the absorption and distortion effects associated with $^2\Sigma$ are rather marked, particularly around the maxima of the curves. The lower one is rather close to the DW results (compare with figure 8), thus showing that in a lower order computational scheme the T matrix does not strongly depend on whether the $f^{(-)}$ orbital is evaluated in the field of the initial or final rotational state. This point is further supported by the plots, in figure 10, of the $\sigma^{DT}(3, 1)$ and $\sigma^{FSC}(3, 1)$ contributions to the total cross section (the σ^{TP} term is too small to appear in the figure). From these results we can say that:

(*a*) the $1 \rightarrow 3$ transition is definitely a one-step process; and

(*b*) the contribution of the FSC term is of minor importance, though not completely negligible, particularly at higher energies ($k^2 \geqslant 0{\cdot}3$ Ryd). These same trends are generally verified for all the $j_i \rightarrow j_i + 2$ processes studied in the present paper, so that we have simply collected them in tables 4–7, where they are compared to the corresponding CC and DW values.

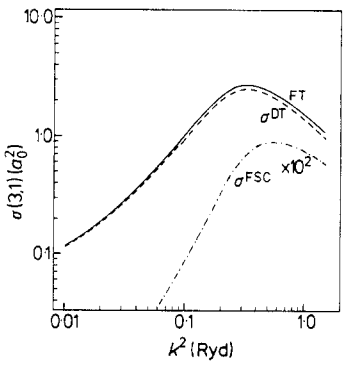

Figure 10. Inelastic $\sigma(3, 1)$ cross sections: the full FT results are compared to the contributions coming from the σ^{DT} and σ^{FSC} cross sections.

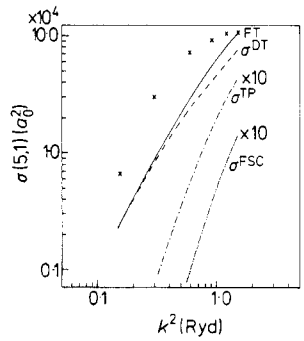

Figure 11. Comparison of the FT and CC $\sigma(5, 1)$ cross sections (full curve and crosses, respectively). Also shown in the figure are the contributions of the single terms in the transition potential.

Table 4. Comparison of the FT, CC and DW $\sigma(2, 0)(a_0^2)$ total cross sections.

k^2(Ryd)	FT	CC	DW
0·03	0·490	0·565	0·495
0·09	1·154	1·479	1·183
0·15	1·904	2·526	1·957
0·3	3·477	4·232	3·422
0·6	3·694	3·810	3·340
0·9	2·864	2·814	2·530
1·2	2·278	2·188	1·763
1·5	1·886	1·803	1·613

Table 5. Comparison of the FT, CC and DW $\sigma(3, 1)(a_0^2)$ total cross sections.

k^2(Ryd)	FT	CC	DW
0·03	0·279	0·314	0·281
0·09	0·871	0·864	0·701
0·15	1·621	1·491	1·175
0·3	2·719	2·526	2·091
0·6	2·179	2·284	2·065
0·9	1·681	1·690	1·565
1·2	1·312	1·314	1·215
1·5	1·073	1·082	0·993

Table 6. Comparison of the FT, CC and DW $\sigma(4, 2)(a_0^2)$ total cross sections.

k^2(Ryd)	FT	CC	DW
0·03	0·277	0·253	0·228
0·09	0·583	0·719	0·587
0·15	1·448	1·260	0·984
0·3	2·337	2·155	1·747
0·6	1·865	1·958	1·725
0·9	1·430	1·449	1·308
1·2	1·115	1·125	1·015
1·5	0·912	0·928	0·829

Table 7. Comparison of the FT, CC and DW $\sigma(5, 3)(a_0^2)$ total cross sections.

k^2(Ryd)	FT	CC	DW
0·03	0·196	0·210	0·196
0·09	0·538	0·648	0·535
0·15	0·916	1·149	0·903
0·3	1·722	1·985	1·616
0·6	1·741	1·810	1·602
0·9	1·326	1·340	1·214
1·2	1·095	1·043	0·941
1·5	0·880	0·858	0·768

We consider next $j_i \to j_i + 4$ inelastic transitions. FT and CC cross sections are compared in figure 11, for the $1 \to 5$ process. In spite of the smallness of the cross section and its rapid variation by two orders of magnitude in a short energy range, the FT curve reproduces the trend of the exact values reasonably well, closely approaching them at higher energies. Also shown in the figures are the contributions of the three terms in the transition potential. A comparison with the corresponding plots of figure 10 shows that the relative weight of σ^{TP} is much higher in the present case than for $j_i \to j_i + 2$ transitions. This would imply that, particularly at higher energies, $1 \to 5$ excitations take place with a strong contribution of the two-step mechanism. At the same time, also, σ^{FSC} is bigger and competitive with σ^{TP}; this fits into the FT physical description of the process, since the impinging electron has now lost a greater amount of energy than in the $1 \to 3$ process. For the sake of completeness, computed values of $\sigma(5, 1)$ and $\sigma(4, 0)$ are collected in table 8.

Table 8. Comparison of the FT and CC values for the $\sigma(4, 0)$ and $\sigma(5, 1)$ total cross sections (in a_0^2).

k^2(Ryd)	$\sigma(4, 0)$	$\sigma(5, 1)$
0·15	4·75(−7)†	2·19(−5)
	1·20(−4)	6·38(−5)
0·3	7·62(−6)	1·08(−4)
	5·26(−4)	2·88(−4)
0·6	9·68(−5)	2·68(−4)
	1·24(−3)	6·87(−4)
0·9	3·66(−4)	4·47(−4)
	1·57(−3)	8·71(−4)
1·2	7·37(−4)	6·67(−4)
	1·79(−3)	9·91(−4)
1·5	1·50(−3)	1·04(−3)
	2·02(−3)	1·12(−3)

† Numbers in parentheses are powers of 10. The upper (lower) number, for each energy, is the FT (CC) value.

5. Conclusions

We have studied in this paper the low energy e^-–H_2 rotational excitation problem, by using a formalism based on effective potentials. The same interaction potential of Lane and Geltman has been adopted, in order to compare with their extensive CC calculations. The present (FT) formalism requires, as the main computational step, the solution of a set of coupled integral equations involving an 'optical' potential. This quantity is, in particular, made up (in our computational scheme) of two terms, one of which is non-local and energy dependent. The number of coupled states which are to be solved for is different from in the CC theory being, among other things, independent of the scattering energy. These aspects have been carefully analysed in the present paper. By solving numerically for this set of equations, it has been verified that elastic processes are strongly dominated by scattering of the electron in the penetrating s-wave states. As such, it has been found that if only the imaginary portion of the non-local term of the optical potential is kept, a better agreement with CC is obtained than if this whole

quantity is used. Inelastic processes are dominated, instead, by higher partial waves and the orbitals describing the impinging and scattered electron are better represented by the full approximation to the second-order term in the optical potential. Consequently, at least for $j_i \rightarrow j_i + 2$ transitions, a very good agreement with CC values is obtained. The present results are generally higher than in the DW approximation, for which explicit calculations have also been carried out. The much smaller $j_i \rightarrow j_i + 4$ cross sections are fairly reproduced by the FT theory, particularly at higher energies. Finally, on the basis of the physical interpretation of the optical and transition potentials of elastic and inelastic scattering, respectively, the present study has shown how it is generally possible to:

(*a*) identify the channels mostly responsible for absorption of energy from the incident beam; and

(*b*) clarify the mechanism by which inelastic transitions take place.

Although the present results seem promising for future applications of the FT theory to the field of low energy electron–molecule scattering, much work has yet to be done before arriving at some definite conclusions. It is probably worth pointing out that while in the present paper a model potential has been adopted (in order to compare with CC computations performed with this interaction) realistic calculations will require accurate forms of the interaction. At this point it can be said that, while the static and long-range polarisation parts of the potential can be readily considered (Faisal 1970, Chandra and Temkin 1976), the exchange portion of the interaction cannot be introduced in an *ab initio* fashion in the present formalism. This does not represent a drawback of the theory, since very accurate phenomenological approximations to exchange are presently available, for both atomic (Bransden *et al* 1976) and molecular (Morrison and Collins 1978) systems.

We are presently considering the task of improving the approximation to the optical potential, so that s waves and, therefore, elastic scattering can be better reproduced. Future work is also planned involving molecules less isotropic than H_2, heteronuclear species and, finally, the very interesting problem of joint vibro-rotational excitations.

References

Arthurs A M and Dalgarno A 1960 *Proc. R. Soc.* A **256** 540–51
Bransden B H, McDowell M R C, Noble C J and Scott T 1976 *J. Phys. B: Atom. Molec. Phys.* **9** 1301–17
Brink D M and Satchler G R 1971 *Angular Momentum* (Oxford: Clarendon Press)
Burke P G and Seaton M J 1971 *Methods in Computational Physics* vol 10 (New York: Academic) pp 1–80
Chandra N and Temkin A 1976 *Phys. Rev.* A **13** 188–203
Csanak Gy, Taylor H S and Ficocelli Varracchio E 1974 *J. Chem. Phys.* **61** 263–70
Faisal F H M 1970 *J. Phys. B: Atom. Molec. Phys.* **3** 636–40
Ficocelli Varracchio E 1977 *J. Phys. B: Atom. Molec. Phys.* **10** 503–13
Lane N F and Geltman S 1967 *Phys. Rev.* **160** 53–67
Morrison M A and Collins L A 1978 *Phys. Rev.* A **17** 918–38
Thomas L D 1973 *J. Comput. Phys.* **3** 348–62
Wang S 1928 *Phys. Rev.* **31** 579–86